

Many-body interactions in a quantum wire in the integer quantum Hall regime: Suppression of the exchange-enhanced g factor

O. G. Balev,^{1,2,*} Sanderson Silva,^{1,3} and Nelson Studart¹

¹*Departamento de Física, Universidade Federal de São Carlos, 13565-905, São Carlos, São Paulo, Brazil*

²*Institute of Semiconductor Physics, National Academy of Sciences of Ukraine, Kiev 03650, Ukraine*

³*Departamento de Física, Universidade Federal do Amazonas, Manaus, Amazonas, Brazil*

(Received 25 May 2005; published 26 August 2005)

The collapse of Hall gaps in the integer quantum Hall liquid in a quantum wire is investigated. Motivated by recent experiment [Pallecchi *et al.*, Phys. Rev. B **65**, 125303 (2002)] previous approaches are extended to treat confinement effects and the exchange-enhanced g factor in quantum wires. Two scenarios for the collapse of the $\nu=1$ state are discussed. In the first one the $\nu=1$ state becomes unstable at $B_{\text{cr}}^{(1)}$, due to the exchange interaction and correlation effects, coming from the edge-state screening. In the second scenario, a transition to the $\nu=2$ state occurs at $B_{\text{cr}}^{(2)}$, with a smaller effective channel width, caused by the redistribution of the charge density. This effect turns the Hartree interaction essential in calculating the total energy and changes $B_{\text{cr}}^{(2)}$ drastically. In both scenarios, the exchange enhanced g factor is suppressed for magnetic fields lower than B_{cr} . Phase diagrams for the Hall gap collapse are determined. The critical fields, activation energy, and optical g factor obtained are compared with experiments. Within the accuracy of the available data, the first scenario is most probable to be realized.

DOI: [10.1103/PhysRevB.72.085345](https://doi.org/10.1103/PhysRevB.72.085345)

PACS number(s): 73.21.Hb, 73.43.Cd, 73.43.Nq, 73.43.Qt

I. INTRODUCTION

Effects of electron-electron interaction and lateral confinement in a two-dimensional electron system (2DES) in the presence of a strong magnetic field B , especially in the integer quantum Hall regime, have attracted significant attention in recent years. Most of the work has been concentrated on the bulk properties of the quantum Hall liquid. However for wide channels of the 2DES, the interplay of the edge states and electron-electron interactions plays a dominant role in the understanding of unusual properties of the Hall liquid.¹⁻⁶ Another system of particular interest, that we focus on in this paper, is the quasi-one-dimensional electron system (Q1DES) in narrow channels hereafter named quantum wires (QWs).⁷⁻¹⁴

It is well known that the bulk Landé g factor that describes the spin splitting in the presence of the magnetic field is strongly affected by many-body interactions and the influence should be more drastic as the dimensionality is reduced. At first glance, the exchange interaction is the main responsible by the enhancement of the g factor at lower dimensions. However, pronounced effects of quantum confinement and electron correlations in QW lead to the proposal of different scenarios in order to understand experimental results.

Kinaret and Lee⁷ found the decreasing of the exchanged spin splitting of a Q1DES in a QW as the width is reduced. By minimizing the total energy, calculated from the unscreened exchange interaction for a fixed linear density n_L , they observed that, at a certain critical density, the exchange enhancement of the spin splitting is suppressed. This phase transition occurs because the cost in the kinetic energy for adding electrons for only one spin-split level increases up to a critical point in which the population of both spin-split levels becomes more favorable for the same n_L .

Only recently the influence of electron correlations coming from the edge states were taken into account.^{5,6,11,12,14} It

was shown that these effects, associated with the strong screening by the edge states, are quite relevant both for QWs (Refs. 11, 12, and 14) and for wide channels.^{5,6,11} For the latter system, Balev and Studart⁵ were able to calculate the screened Coulomb potential by performing an exact infinite summation of a power series in the relevant parameter $r_0 = e^2/\epsilon l_0 \hbar \omega_c$ which characterizes the strength of the electron-electron interaction relative to the cyclotron energy. Here $l_0 = \sqrt{\hbar/m^* \omega_c}$ is the magnetic length, $\omega_c = |e|B/m^*c$ the cyclotron frequency, and ϵ is the background dielectric constant. In the Balev-Studart (BS) self-consistent nonlocal treatment, the many-particle energy dispersion relations are obtained from the solution of a single-particle Schrödinger equation determined by an exchange-correlation potential which is given in terms of the total single-particle energy and the effective confining potential.¹⁵ The latter one is calculated in the self-consistent Hartree approximation (HA) taking into account screening effects on the external (bare) one-electron lateral confining potential.⁵ The BS approach has the merit that, by considering infinite number of terms in a systematic expansion in powers of $r_0 \ll 1$, its validity is well justified for $r_0 \lesssim 1$ (in experiments $r_0 \sim 1$) and for different confining potentials provided their forms are smooth on the l_0 scale. If we adopt the parabolic confinement $V_y = m^* \Omega^2 y^2 / 2$, where Ω is the confinement frequency, that implies $\Omega^2 / \omega_c^2 \ll 1$. It was shown that edge-state nonlocal correlations change appreciably the spectrum of the spin-split Landau levels (LLs) leading to a highly asymmetric Fermi level within the gap between the ($n=0, \sigma=+1$) and ($n=0, \sigma=-1$) LLs as well the edge group velocity is drastically renormalized. As further conclusions, it was shown in BS that the strong correlation effects induced by the edge states can lead to the collapse of the fundamental Hall gap, which defines the activation g factor. As these findings are noticeable, we cannot neglect exchange-correlation effects in calculating many-body prop-

erties of the $\nu=1$ quantum Hall liquid in electron channels.

In this paper, the BS approach is extended to determine the structure of lowest spin-split LLs ($n=0$, $\sigma=\pm 1$) in the QW system for the $\nu=1$ quantum Hall liquid at zero temperature. Here the parameter ν for the QW is defined, as usual, as the filling factor of the LLs at the center of the QW. Strong correlation effects due to the screening of both left and right edges of the channel are now taken fully into account. In addition to the intrinsic interest on theoretical aspects of this intensively studied system, our motivation stems mainly from recent magnetocapacitance experiment in GaAs/AlGaAs QW heterostructures where the evolution 1D subband filling and spacing was studied as function of confinement, gate voltage and magnetic field.¹³ In this reference, Pallecchi *et al.* compared the experimental results with the predictions by Kinaret and Lee⁷ and by Balev and Vasilopoulos¹¹ and concluded that essential improvements of these models are needed.

We obtain analytically the renormalized, by exchange-correlation effects, group velocity $v_{g0}^{(1)}$ of the edge states and find that $v_{g0}^{(1)} \propto (v_{g0}^{1,H})^{1/2}$, where $v_{g0}^{1,H}$ is the edge-state group velocity in the HA. We calculate also the enhanced activation gap G , strongly dependent on the exchange-correlation interaction, for several values of the magnetic field and the Fermi wave vector k_F , which defines the width W of the QW because W is linearly proportional to the number of filled k states for a given band. Similarly to the wide channel system, we show that the spatial behavior of the occupied LL in a QW is strongly modified due to electron correlations, especially near the edges, in comparison with the results in the HA and the Hartree-Fock approximation (HFA). The position of the Fermi level in the gap at the center of the QW is highly asymmetric due to correlation effects induced by edge states. Though in the HFA, the exchange interaction leads to the edge-state velocity $v_{g0}^{1,x}$ that diverges logarithmically, correlation effects restore the smoothness of the single-particle energy as a function of the oscillator center y_0 , on the l_0 scale.^{5,11,12}

In order to understand better the effects of electron-electron interaction and lateral confinement on the exchange-enhanced spin splitting at the $\nu=1$ Hall state in QW, we treat two scenarios for the collapse of the activation gap G . In the first one, there is no change in the effective QW width when the $\nu=1$ state becomes unstable at a critical magnetic field $B_{cr}^{(1)}$. As a consequence, no finite redistribution of the electron charge density occurs at $B_{cr}^{(1)}$, when the Fermi level touches the bottom of empty LL ($n=0$, $\sigma=1$). This scenario, proposed in Ref. 11, is analyzed here by employing the BS approach to study the energy spectrum, activation gap and “optical” g factor of the QW. In the second scenario, similar to that discussed by Kinaret and Lee,⁷ we include the very essential Hartree energy, missed in Ref. 7. Now the transition to the $\nu=2$ state happens at a certain $B_{cr}^{(2)}$. For $B < B_{cr}^{(2)}$, in the $\nu=1$ state, the increase of the kinetic energy exceeds the energy gain from the exchange energy plus the Hartree energy, with respect to the $\nu=2$ state, such that the total energy of the QW in the $\nu=2$ state is lower than in $\nu=1$ state. In this scenario, the width of the QW becomes two times smaller (if we neglect the bare g factor g_0) for $B < B_{cr}^{(2)}$. We make a

detailed analysis of both scenarios and compare their predictions with experimental results^{10,13} as well as with the predictions of Kinaret and Lee model.⁷ We show that the first scenario is realized in experimentally observed collapse of the activation gap of the $\nu=1$ quantum Hall state as in wide channels of Ref. 10 ($W \sim 3000$ Å, $\hbar\Omega \sim 0.5$ meV) as for much narrower QWs considered in recent experiment by Pallecchi *et al.* ($W \sim 500$ Å, $\hbar\Omega \sim 5$ meV).¹³

The outline of our paper is as follows. In Sec. II A, we extend, for a sake of completeness, on QWs the microscopic formalism of Ref. 5 for obtaining the screened Coulomb interaction in the very strong magnetic field limit $r_0 \ll 1$. In Sec. II B, the BS approach, for $r_0 \lesssim 1$, is extended for the quantum Hall liquid in the QW. We calculate the structure of the LL subband dispersion, the renormalization, due to exchange and correlations, of the group velocity of edge states, the activation gap and the optical g factor. The first scenario of the $\nu=1$ collapse is discussed. In Sec. III A, we revisit the Kinaret-Lee model and discuss the second scenario for the suppression of the $\nu=1$ state spin splitting within the HFA. A detailed comparison of our results for phase transitions from both scenarios with the experimental results of Refs. 10 and 13 as well with those from the model of Ref. 7 is provided in Sec. III B. We summarize the key results and present our conclusions in Sec. IV.

II. EXCHANGE-CORRELATION EFFECTS IN THE QUANTUM WIRE AT $\nu=1$

We consider the Q1DES in a QW of width W and length $L_x=L$ lying in the (x,y) plane in the presence of a strong magnetic field B pointing up along the z axis. Choosing the vector potential $\mathbf{A} = -By\hat{x}$, the single-particle Hamiltonian in the HA is given as $\hat{h}^0 = [(\hat{p}_x + eBy/c)^2 + \hat{p}_y^2]/2m^* + V_y + g_0\mu_B\hat{\sigma}_z B/2$, where the confining potential $V_y = m^*\Omega^2 y^2/2$, g_0 is the bare Landé g factor, μ_B the Bohr magneton, and $\hat{\sigma}_z$ the z component Pauli matrix. The eigenvalues and eigenfunctions are given by $\epsilon_{n,k_x,\sigma} = (n+1/2)\hbar\tilde{\omega} + \hbar^2 k_x^2/2\tilde{m} + \sigma g_0\mu_B B/2$ and $\psi_{n,k_x,\sigma}(\mathbf{r}, \sigma_1) = \langle \mathbf{r} | nk_x \rangle | \sigma \rangle$, with $\langle \mathbf{r} | nk_x \rangle = \exp(ik_x x) \Psi_n[y - y_0(k_x)]/\sqrt{L}$ and spin function $|\sigma\rangle = \psi_\sigma(\sigma_1) = \delta_{\sigma\sigma_1}$, $\sigma_1 = \pm 1$. Here $\tilde{\omega} = (\omega_c^2 + \Omega^2)^{1/2}$, $\tilde{m} = m^* \tilde{\omega}^2/\Omega^2$, $y_0(k_x) = \hbar\omega_c k_x/m^* \tilde{\omega}^2$, $\Psi_n(y)$ is a harmonic oscillator function.

For the $\nu=1$ quantum Hall liquid in the HA the right (left) edge of the occupied ($n=0$, $\sigma=1$) LL is denoted by $y_{r0}^{(1)} = \hbar\omega_c k_F/m^* \tilde{\omega}^2 (-y_{r0}^{(1)})$, where $k_F = (\tilde{\omega}/\hbar\Omega) \sqrt{2m^* \Delta_{F0}^{(1)}}$ is the Fermi vector; this level is occupied only for $|k_x| \leq k_F$, $\Delta_{F0}^{(1)} = E_F^H - \hbar\tilde{\omega}/2 - g_0\mu_B B/2$, and E_F^H is the Fermi energy in the HA. The QW width is $W = 2y_{r0}^{(1)}$. The group velocity of the edge states in the HA, at the right (left) edge of the QW is given by $v_{g0}^{1,H} = \partial\epsilon_{0,k_F,1}/\hbar\partial k_x = \hbar k_F/\tilde{m} (-\hbar k_F/\tilde{m})$.

For the parabolic confinement, the essential matrix elements were evaluated in Ref. 11. The result is

$$\begin{aligned} \langle n' k'_x | e^{iq_x \mathbf{r}} | nk_x \rangle &= \langle n' k'_x | e^{iq_x y} | nk_x \rangle \delta_{q_x, -k_-} \\ &= \left(\frac{n'!}{n!} \right)^{1/2} \left(\frac{aq_x + iq_y}{\sqrt{2}\tilde{l}} \right)^m e^{-u/2} \\ &\quad \times L_n^m(u) e^{iaq_x k_x \tilde{l}^2/2} \delta_{q_x, -k_-}, \end{aligned} \quad (1)$$

where $k_{\pm} = k_x \pm k'_x$, $m = n - n'$, $a = \omega_c / \tilde{\omega}$, $u = [a^2 q_x^2 + q_y^2] \tilde{l}^2 / 2$, $\tilde{l} = (\hbar / m^* \tilde{\omega})^{1/2}$ is the renormalized magnetic length, and $L_n^m(u)$ the Laguerre polynomial. Observe that the Eq. (7) of Ref. 7 differs from Eq. (1) and the \mathbf{q} anisotropy of $\langle n' k'_x | e^{i\mathbf{q}\cdot\mathbf{r}} | n k_x \rangle$ should be pointed out especially for $\omega_c / \Omega \lesssim 1$.

A. Many-body interactions for $r_0 \ll 1$

We will now consider exchange-correlation effects in the QW for the strong magnetic field limit, $r_0 \ll 1$, when only the lowest spin-up ($\sigma = +1$) LL is occupied. The exchange and correlation contributions to the single-particle energy of this LL $E_{0,k_x,1} = \epsilon_{0,k_x,1} + \epsilon_{0,k_x,1}^{xc}$ in the screened Hartree-Fock approximation (SHFA) is given as¹¹

$$\begin{aligned} \epsilon_{0,k_x,1}^{xc} = & -\frac{1}{8\pi^3} \int_{-k_F}^{k_F} dk'_x \int_{-\infty}^{\infty} dq_y \int_{-\infty}^{\infty} dq'_y V^s(k_-, q_y; q'_y) \\ & \times (0k_x | e^{iq_x y} | 0k'_x) (0k'_x | e^{iq'_x y} | 0k_x), \end{aligned} \quad (2)$$

where $V^s(q_x, q_y; q'_y)$ is the Fourier transform of the screened Coulomb interaction which can be evaluated within the random phase approximation (RPA). For comparison with experiments,^{10,13} we will assume further in Sec. II that $\Omega^2 / \omega_c^2 \ll 1$, then $\tilde{l} \approx l_0 = (\hbar / m^* \omega_c)^{1/2}$.

In order to calculate the screened Coulomb interaction, we follow closely Ref. 5. The integral equation for the Fourier components of the induced charge density, by the test electron charge located at (x_0, y_0) , is given as

$$\begin{aligned} \rho(q_x, y; y_0) = & -r_1^H \sum_{k=0}^1 \Pi_{00}[y, (-1)^k k_F, (-1)^k k_F - q_x] \\ & \times \int_{-\infty}^{\infty} d\tilde{y} \int_{-\infty}^{\infty} dy' K_0(|q_x| |\tilde{y} - y'|) \\ & \times \Pi_{00}(\tilde{y}, (-1)^k k_F, (-1)^k k_F - q_x) \\ & \times [\rho(q_x, y'; y_0) + e \delta(y' - y_0)], \end{aligned} \quad (3)$$

where $k=0$ (1) term is related to the contribution coming from the right (left) edge states, $r_1^H = e^2 / (\pi \hbar \epsilon v_{g0}^{1,H})$ is a characteristic dimensionless parameter, $\Pi_{n_\alpha n_\beta}(y, k_{x\alpha}, k_{x\beta}) = \Psi_{n_\alpha}[y - y_0(k_{x\alpha})] \Psi_{n_\beta}[y - y_0(k_{x\beta})]$, and $K_0(x)$ is the modified Bessel function. Equation (3) is similar to Eq. (4) of Ref. 5. However, notice the essential point that two terms are now present in Eq. (3) because one cannot neglect contributions from both left and right edges at any point of the QW.

We look for a solution of Eq. (3) in the form

$$\rho(q_x, y; y_0) = \sum_{k=0}^1 \rho^{(k)} \Pi_{00}[\tilde{y}, (-1)^k k_F, (-1)^k k_F - q_x], \quad (4)$$

where $\rho^{(k)} \equiv \rho^{(k)}(q_x, y_0)$. Substituting the Eq. (4) into Eq. (3), we obtain the system of two linear inhomogeneous equations with respect to $\rho^{(k)}(q_x, y_0)$, for $k=0, 1$. Calculating these functions and then taking the Fourier transform $\rho(q_x, q_y; q'_y)$ of $\rho(q_x, y; y_0)$ it follows from $V^s(q_x, q_y; q'_y) = (2\pi e / \epsilon \sqrt{q_x^2 + q_y^2}) [2\pi e \delta(q_y + q'_y) + \rho(q_x, q_y; q'_y)]$ that

$$\begin{aligned} V^s(q_x, q_y; q'_y) = & \frac{4\pi^2 e^2}{\epsilon \sqrt{q_x^2 + q_y^2}} \left\{ \delta(q_y + q'_y) \right. \\ & - \frac{r_1^H \exp[iq_x(q_y + q'_y)l_0^2/2]}{\Delta^H(q_x) \sqrt{q_x^2 + (q'_y)^2}} \\ & \times e^{-[2q_x^2 + q_y^2 + (q'_y)^2]l_0^2/4} \{ [1 + r_1^H M(0, q_x)] \\ & \times \cos[k_F(q_y + q'_y)l_0^2] - r_1^H M(2k_F, q_x) \\ & \left. \times \cos[k_F(q_y - q'_y)l_0^2] \right\}, \end{aligned} \quad (5)$$

where

$$M(k_x, q_x) = e^{-q_x^2 l_0^2/2} \int_0^{\infty} dq_y \frac{e^{-q_y^2 l_0^2/2}}{\sqrt{q_x^2 + q_y^2}} \cos[q_y k_x l_0^2], \quad (6)$$

and

$$\Delta^H(q_x) = [1 + r_1^H M(0, q_x)]^2 - [r_1^H M(2k_F, q_x)]^2. \quad (7)$$

From Eq. (6) it follows that $M(0, q_x) = 2^{-1} \exp \times (-q_x^2 l_0^2/4) K_0(q_x^2 l_0^2/4)$ and for $2k_F l_0 \gg 1$, $M(2k_F, q_x) \approx K_0(2k_F q_x l_0^2)$. The first term in the curly brackets of Eq. (5) is the bare Coulomb interaction which leads to the exchange contribution,^{3,7,11} with neglected small corrections of the order of $\Omega^2 / \omega_c^2 \ll 1$.

Substituting Eq. (5) into Eq. (2), we obtain the single-particle exchange-correlation energy as

$$\begin{aligned} \epsilon_{0,k_x,1}^{xc} = & -\frac{e^2}{\pi \epsilon} \int_{-k_F}^{k_F} \frac{dk'_x}{\Delta^H(k_x - k'_x)} \left\{ M(0, k_x - k'_x) \Delta^H(k_x - k'_x) \right. \\ & - r_1^H \left\{ [1 + r_1^H M(0, k_x - k'_x)] \times \sum_{k=0}^1 M^2[k_x + (-1)^k k_F, k_x \right. \\ & \left. - k'_x] - 2r_1^H M(2k_F, k_x - k'_x) M(k_x - k_F, k_x - k'_x) \right. \\ & \left. \left. \times M(k_x + k_F, k_x - k'_x) \right\} \right\}. \end{aligned} \quad (8)$$

The first term in the curly brackets of Eq. (8) gives the exchange energy. Remaining terms are the important electron-correlation contributions to the energy coming from the edge-state screening of both left and right edges of the QW.

B. Structure of Landau level subbands for $r_0 \lesssim 1$

In order to make comparisons between theoretical predictions and the results of actual experiments, it is necessary to go beyond the strong magnetic field limit ($r_0 \ll 1$), considered in Sec. II A, to reach the regime achieved experimentally ($r_0 \sim 1$). We begin by defining a new characteristic dimensionless parameter $r_1 = e^2 / (\pi \hbar \epsilon v_{g0}^{(1)})$ instead of r_1^H and assuming that the approximation is still valid for $r_0 \lesssim 1$. Then the total single-particle energy of the ($n=0, \sigma=1$) LL $E_{0,k_x,1} = \epsilon_{0,k_x,1} + \epsilon_{0,k_x,1}^{xc}$, where $\epsilon_{0,k_x,1}^{xc}$ is given by Eq. (8), is given by

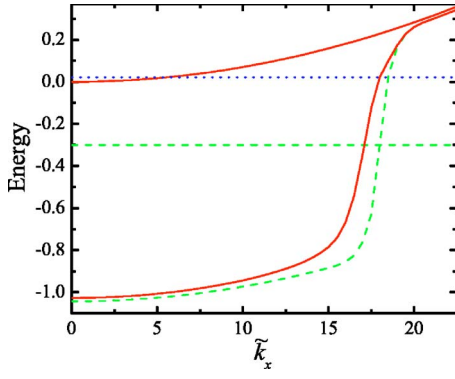


FIG. 1. (Color online.) Energy dispersion curves for the lowest levels of the quantum wire (units of $\hbar\omega_c$) as a function of $\tilde{k}_x = k_x l_0$. The bottom (top) red solid line represents $E_{0,k_x,1}$ ($E_{0,k_x,-1}$) and the blue dot horizontal line gives the exact position of E_F , when exchange-correlation effects are taken into account in the BS approach. The green dashed curve shows $E_{0,k_x,1}$ obtained within the HFA. The horizontal green dashed line indicates the position of the Fermi level E_F within the HFA. The used parameters are $B=10$ T, $\hbar\Omega=0.65$ meV, and $k_F l_0=18.0$ ($W \approx 0.29$ μm), which correspond to parameters of sample 1 in Ref. 10. Here $r_0 \approx 0.82$, $\omega_c/\Omega \approx 26.6$, $\delta=10^{-3}$, and $v_g/v_g^H \approx 8.5$. As for these conditions the activation gap is negative ($G_a \approx -2.9$), there is no stable $\nu=1$ QHE state, in agreement with experiment (Ref. 10) and, respectively, here the blue dot line actually indicates the quasi-Fermi level.

$$E_{0,k_x,1} = \frac{\hbar\omega_c}{2} - \frac{|g_0|\mu_B B}{2} + \frac{m^* \Omega^2 l_0^4}{2} k_x^2 - \frac{e^2}{\pi\epsilon} \times \int_{-k_F - k_x}^{k_F - k_x} \frac{dx}{\Delta(x_\delta)} \{M(0, x_\delta) \Delta(x_\delta) - r_1 \{ [1 + r_1 M(0, x_\delta)] \times [M^2(k_x - k_F, x_\delta) + M^2(k_x + k_F, x_\delta)] - 2r_1 M(2k_F, x_\delta) \times M(k_x - k_F, x_\delta) M(k_x + k_F, x_\delta) \} \}, \quad (9)$$

where $x_\delta = \sqrt{x^2 + \delta^2/l_0^2}$, $\Delta(x)$ it follows from $\Delta^H(x)$ after changing r_1^H by $r_1 \equiv r_1(v_{g0}^{(1)})$. The renormalized group velocity of the edge states is defined from Eq. (9) as $v_{g0}^{(1)} = (\partial E_{0,k_x,1} / \hbar \partial k_x)_{k_x=k_F}$. This is the condition of self-consistency in the BS approach for the QW. Renormalized by exchange-correlation effects, $v_{g0}^{(1)}$ is given by a positive solution of the cubic equation

$$\tilde{v}_g^3 + [M(0, \delta/l_0) - \tilde{v}_g^H] \tilde{v}_g^2 - 2\tilde{v}_g^H M(0, \delta/l_0) \tilde{v}_g - \tilde{v}_g^H [M^2(0, \delta/l_0) - M^2(2k_F, \delta/l_0)] = 0, \quad (10)$$

where $\tilde{v}_g = 1/r_1$, $\tilde{v}_g^H = 1/r_1^H$. This equation was calculated by using $[\partial M(k_x - k_F, x_\delta) / \partial k_x]_{k_x=k_F} = 0$ and for assumed restriction $2k_F l_0 \gg 1$. A small parameter $\delta \ll 1$ was introduced in order to avoid the weak logarithmic divergence for $x \rightarrow 0$. Here $M(0, \delta/l_0) \approx [\ln(2\sqrt{2}/\delta) - \gamma/2]$ and $M(2k_F, \delta/l_0) \approx K_0(2k_F l_0 \delta) \approx [\ln(1/k_F l_0 \delta) - \gamma]$, where γ is the Euler constant and $2k_F l_0 \delta \ll 1$. It is worth to point out that by formally discarding the terms containing $M^2(2k_F, \delta/l_0)$ of Eq. (10), which corresponds to neglect the correlations due to left edge-states of the QW, the Eq. (14) of Ref. 5 is obtained. From Eq. (10) for the condition $\tilde{v}_g^H \ll [\ln(8k_F^2 l_0^2) + \gamma]$, which is

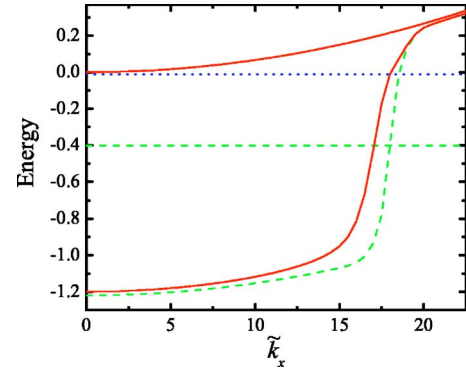


FIG. 2. (Color online.) Same as in Fig. 1 for the parameters pertinent to sample 2 of Ref. 10: $B=7.3$ T, $\hbar\Omega=0.46$ meV, and $k_F l_0=18.0$ ($W \approx 0.34$ μm). Now $r_0 \approx 0.96$, $\omega_c/\Omega \approx 27.4$, $v_g/v_g^H \approx 9.45$ and the activation gap is positive ($G_a \approx 1.53 > 0$) leading to a stable $\nu=1$ QHE state in the QW, in agreement the experimental result (Ref. 10) in which $G_a \approx 1.0$.

well satisfied for the assumptions made, we find that only one root

$$v_{g0}^{(1)} = \sqrt{\frac{e^2}{\pi\hbar\epsilon}} v_{g0}^{1,H} \{ [M^2(0, \delta/l_0) - M^2(2k_F, \delta/l_0)] \times M^{-1}(0, \delta/l_0) \}^{1/2} + v_{g0}^{1,H} \approx \sqrt{\frac{e^2}{\pi\hbar\epsilon}} v_{g0}^{1,H} [\ln(8k_F^2 l_0^2) + \gamma]^{1/2} + v_{g0}^{1,H}, \quad (11)$$

satisfies the physical requirement of $v_{g0}^{(1)} \geq 0$, i.e., the occupied LL is below E_F within the interval $(-k_F, k_F)$. From Eq. (11) it follows that $v_{g0}^{(1)}/v_{g0}^{1,H} \approx \{ r_1^H [\ln(8k_F^2 l_0^2) + \gamma] \}^{1/2} \gg 1$ and we finally obtain $v_{g0}^{(1)} \propto \sqrt{v_{g0}^{1,H}}$. Note that the approximate expression in Eq. (11), is independent of the small parameter δ , contrary to the result obtained for wide channels.⁵ Our Eq. (11) is essentially different from Eq. (21) of Ref. 12 that gives $v_{g0}^{(1)} \approx v_{g0}^{1,H}$, for $r_0 \leq 1$. If we apply Eq. (11) to the actual parameters of samples 1 and 2 of Ref. 10 it follows that $v_{g0}^{(1)}/v_{g0}^{1,H} \approx 10.4$ (9.1) and 19.6 (17.0) for $\delta \rightarrow 0$ ($\delta=10^{-3}$), respectively. In Ref. 11 it was found $v_{g0}^{(1)}/v_{g0}^{1,H} \approx 5$ and 10 for samples 1 and 2, at $\delta=10^{-3}$. On the other hand, these ratios were calculated numerically by a weighted iterative method in Ref. 12 and the values obtained are $v_{g0}^{(1)}/v_{g0}^{1,H} \approx 6.9$ and 11 which are close to our results and in contrast with the analytical result $v_{g0}^{(1)}/v_{g0}^{1,H} \approx 1.0$, for $r_0 \leq 1$, given in Refs. 12 and 14. The last line in Eq. (11) can be rewritten as $v_{g0}^{(1)}/v_{g0}^{1,H} = \sqrt{r_0/\pi} (\omega_c/\Omega) \{ [\ln(8k_F^2 l_0^2) + \gamma] / k_F l_0 \}^{1/2} + 1$, for a parabolic V_y . However, Eqs. (10) and (11) are valid for any confining potential V_y that satisfies the condition of smoothness on l_0 scale. For instance we can assume here large variation of $v_{g0}^{1,H}$ for a fixed $W=2k_F l_0$. In particular, $v_{g0}^{1,H}$ can approach zero due to the flattening effect,¹ while $W/l_0=2k_F l_0 \gg 1$ is kept constant.

The activation gap, defined by the energy difference between the bottom of ($n=0, \sigma=-1$) LL and the Fermi level, is given by $G(v_{g0}^{1,H}) = E_{0,0,-1} - E_{0,k_F,1} = \epsilon_{0,0,-1} - E_{0,k_F,1}$, where the

Fermi level $E_F = E_{0,k_F,1}$ follows from Eqs. (9)–(11). The result is

$$G = |g_0| \mu_B B - \frac{m^* \omega_c^2}{2\Omega^2} (v_{g_0}^{1,H})^2 + \frac{e^2}{\pi \epsilon l_0} \int_0^{2k_F l_0} du \{M(0, u \delta / l_0) \times [1 + R_1 M(0, u \delta / l_0)] - R_1 \times M^2(2k_F, u \delta / l_0)\} \{ [1 + R_1 M(0, u \delta / l_0)]^2 - R_1^2 M^2(2k_F, u \delta / l_0) \}^{-1}, \quad (12)$$

where $R_1 \equiv R_1(v_{g_0}^{1,H})$ is the function obtained from $r_1(v_{g_0}^{(1)})$, after using the solution $v_{g_0}^{(1)} = v_{g_0}^{(1)}(v_{g_0}^{1,H})$ of Eq. (10) and $u_\delta = \sqrt{u^2 + \delta^2}$. Notice that due to the terms depending on $M(2k_F, \delta / l_0)$, Eq. (12) is essentially different from Eq. (16) of Ref. 5. We emphasize that the edge-state correlation effects constrain the Fermi level of the interacting system at the center of the QW to be much closer to the bottom of the empty ($n=0, \sigma=-1$) LL than to the bottom of the occupied ($n=0, \sigma=1$) LL. For instance, observe the position of E_F in Figs. 2 and 3 at the central part of QW, $k_x/k_F \ll 1$. Then we must say that G is the actual activation gap of the QW.

In order to assess the effect of many-body interactions on G , we define a dimensionless activation gap as $G_a(v_{g_0}^{1,H}) = G / (|g_0| \mu_B B / 2)$.⁵ In the absence of many-body interactions, i.e., in HA the maximum value of G_a will be achieved if $\Omega \rightarrow 0$ and E_F^H is exactly in the middle of the Fermi gap at $k_x=0$, $G_{a \max} \equiv G_{a \max}^H = 1$. Then the activation gap is enhanced when $G_a > 1$. Indeed G_a can be understood as the activation g factor of the QW given in units of the bare g factor g_0 . We see that a critical magnetic field $B_{cr}^{(1)}$ is achieved when $G_a = 0$. For $B > B_{cr}^{(1)}$ we have $G_a > 0$ and the $\nu=1$ state is thermodynamically stable. Otherwise for $B < B_{cr}^{(1)}$, $G_a < 0$ and the $\nu=1$ state is unstable. Furthermore, Pallecchi *et al.*¹³ were able to obtain the value of “optical” g factor $g_{op}^* = (E_{0,k_x,-1} - E_{0,k_x,1}) / \mu_B B$ for $k_x=0$. Notice, in agreement with experiment, that $g_{op}^*(k_x)$ can be large, due to the exchange enhancement, even when G_a goes to 0.

The energy spectra of the spin-split LL subbands calculated within the BS approach and within the Hartree-Fock approximation, where no correlation effects are included, are depicted in Fig. 1. Horizontal lines represent the position of the Fermi level E_F obtained from both methods. The parameters used in calculations are those for sample 1 of Ref. 10. We see that for these values $r_0 \approx 0.82$, $\omega_c / \Omega \approx 26.6$, and $v_g / v_g^H \approx 8.5$, the criterion of validity of the BS approach is fulfilled and, because the activation gap is negative ($G_a \approx -2.9$), any stable $\nu=1$ quantum Hall effect (QHE) state does exist in agreement with experiment.¹⁰ As shown in Fig. 1, in the BS approach, E_F is actually the quasi-Fermi level when $G_a < 0$.

In Figs. 2 and 3 we show the calculation results for the pertinent parameters of the sample 2 of Ref. 10. In Fig. 2 we took the most probable experimental values of $\hbar\Omega = 0.46$ meV and $W \approx 0.34$ μm , and now the magnetic field $B = 7.3$ T which leads to $r_0 \approx 0.96$, $\omega_c / \Omega \approx 27.4$, $v_g / v_g^H \approx 9.45$. We find that now G_a is positive ($G_a \approx 1.53$) and close to the experimental value $G_a \approx 1.0$ which corresponds to the existence of a stable $\nu=1$ QHE state in this sample.¹⁰ Figure 3 exhibits the spin-split LL subbands for another confine-

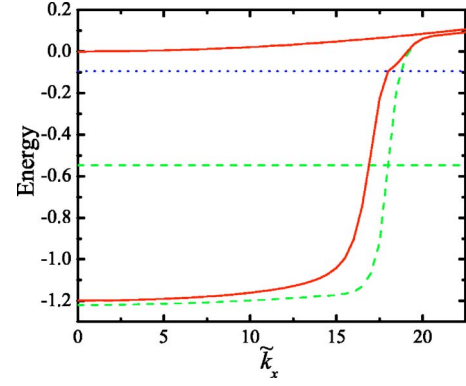


FIG. 3. (Color online.) Same as in Fig. 2 for the confining frequency $\hbar\Omega = 0.26$ meV, which corresponds to the estimated threshold for sample 2 in Ref. 10. Here $\omega_c / \Omega \approx 48.5$, where $v_g / v_g^H \approx 16.2$ and $G_a \approx 12.9$.

ment frequency $\hbar\Omega = 0.26$ meV (the estimated threshold value in¹⁰ for sample 2). In this case $\omega_c / \Omega \approx 48.5$, where $v_g / v_g^H \approx 16.2$, and $G_a \approx 12.9$. Again a stable the QHE state is predicted to exist.

The dimensionless activation gap G_a is shown in Fig. 4 as a function of the HA group velocity calculated within the BS approach for $B = 10.0$ and 7.3 T. The points (\tilde{v}_g^H, G_a) pertinent to parameters of Figs. 1–3 are represented by the square, circle, and triangle marks. They indicate the collapse of the $\nu=1$ state (square) or its stability (circle and triangle) for the QWs in the samples of Ref. 10.

Now we focus on the results, obtained within the BS approach for the QWs, pertinent to more recent experimental work of Pallecchi *et al.*¹³ In Fig. 5 we plot the effective, spatially inhomogeneous, “optical” g factor g_{op}^* as a function of \tilde{k}_x for $B = 14.0$ T, $\hbar\Omega = 4.75$ meV which corresponds to the weakest lateral confinement in the experiment, at $V_{\text{side}} = 0$; $\delta = 10^{-3}$. The chosen parameters $k_F l_0$ correspond to QW

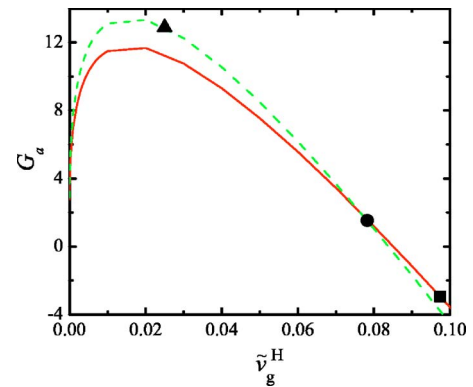


FIG. 4. (Color online.) Dimensionless activation gap G_a , or activation gap G in units of $|g_0| \mu_B B / 2$, for the $\nu=1$ state, as a function of the HA group velocity \tilde{v}_g^H , calculated within the BS scheme for $k_F l_0 = 18.0$ and $\delta = 10^{-3}$. The red solid and green dashed curves correspond to $B = 10.0$ and 7.3 T, respectively. The square mark ($G_a \approx -2.94$, indicating the collapse of the $\nu=1$ state) corresponds to Fig. 1 parameters. The point marked by the circle (triangle) corresponds to Figs. 2 (3) and it $G_a \approx 1.53$ (12.9) clearly predicts the existence of the $\nu=1$ QHE state in this QW sample.

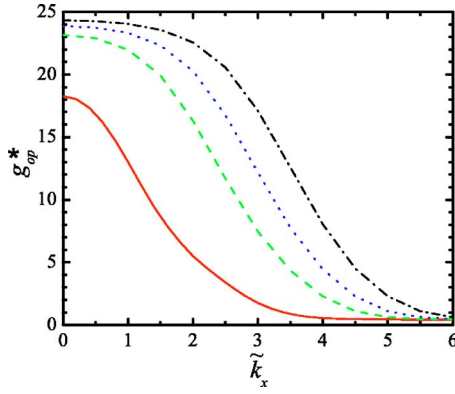


FIG. 5. (Color online.) Effective “optical” g_{op}^* as a function of \tilde{k}_x , for the experimental conditions of Ref. 13: $B = 14.0$ T, $\hbar\Omega = 4.75$ meV. The red solid, green dashed, blue dotted, and black dash-dotted curves are depicted for $k_{F0} = 1.83, 3.0, 3.5,$ and 4.0 corresponding to linear density $n_L = 8.5 \times 10^5, 1.39 \times 10^6, 1.63 \times 10^6,$ and 1.87×10^6 cm $^{-1}$, respectively. The values of the $g_{\text{op}}^* \approx 18.3, 23.2$ and 23.9 at $\tilde{k}_x = 0$ for the solid, dashed and dotted curves are very close to the measured value $g_{\text{op}}^* \approx 21$. The red solid curve corresponds to effective QW width $W \approx 250$ Å.

widths smaller than the nominal lithographic width (~ 1500 Å), the upper limit for the effective QW width W . Typical values for the g factor at $\tilde{k}_x = 0$ $g_{\text{op}}^* \approx 18.3, 23.2,$ and 23.9 from the solid, dashed, and dotted curves are rather close to the measured value ($g_{\text{opt}}^* \approx 21$, see Fig. 5 of Ref. 13). We point out that the existence of the $\nu = 1$ state in the QW is not predicted only for the parameters used for calculation of the dash-dotted curve. In Fig. 5 the requirements for the applicability of the BS approach for the QW are well fulfilled; $r_0 \approx 0.69$, $\omega_c/\Omega \approx 5.1$ and on the average, $v_g/v_g^H \approx 1.0$, $\tilde{v}_g^H < 1.0$. In Fig. 6 dimensionless activation gap G_a is plotted as a function of \tilde{v}_g^H (here it is $\propto \Omega^2/\omega_c^2$) calculated within the BS approach for $B = 14.0$ T. The curves are shown for the

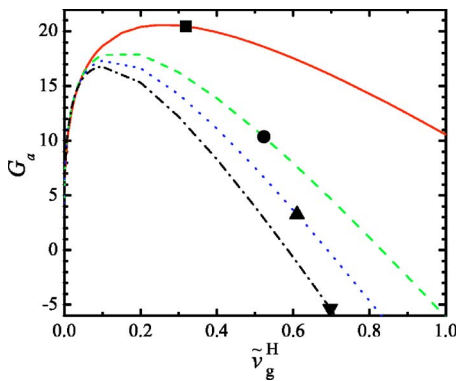


FIG. 6. (Color online.) Dimensionless activation gap G_a as a function of \tilde{v}_g^H (or Ω^2/ω_c^2) calculated within the BS scheme for $B = 14.0$ T and $\nu = 1$. The red solid, green dashed, blue dotted, and black dash-dotted curves were calculated for the same values of k_{F0} and W as given in Fig. 5. The square, circle, triangle, and inverse-triangle symbols indicated the values of G_a for $\hbar\Omega = 4.75$ meV (or $\omega_c/\Omega \approx 5.1$), used in Fig. 5. It is seen that the inverse-triangle mark ($G_a = -5.35$) implies the collapse of the $\nu = 1$ state.

same parameters as in Fig. 5. However, in contrast with Fig. 5, Ω is now a variable parameter.

III. COLLAPSE OF THE $\nu = 1$ QUANTUM HALL STATE IN THE QUANTUM WIRE

We now turn to the important question of collapse of the $\nu = 1$ QHE state in a QW, due to the suppression of exchange-enhanced spin splitting for the two different theoretical scenarios of the collapse, or the phase transition, which we propose to understand the experimental findings. In the first one, there is no change in the QW width at $B_{\text{cr}}^{(1)}$, when the Fermi level E_F reaches the bottom of ($n=0, \sigma=1$) LL. This scenario is developed here by employing the BS self-consistent approach (beyond the HFA), as discussed in Sec. II. The second scenario is similar to one proposed by Kinaret and Lee, where the collapse of the $\nu = 1$ state is caused by the transition to the $\nu = 2$ state in the centre of the QW. The latter state has an effective width two times smaller than the former one if we ignore the bare g factor; $g_0 = -0.44$ for GaAs samples. For a more accurate description of this phase transition some improvements in the study of Ref. 7, discussed partly in Sec. I, are necessary.

A. Collapse of the state within the second scenario

We will not restrict ourselves, in this subsection, to the limit $\Omega^2/\omega_c^2 \ll 1$, but consider also the important case $\Omega/\omega_c \geq 1$, by using Eqs. (1) and (2) and other general formulas of Sec. II valid for arbitrary Ω/ω_c . Within the restricted HFA model the single-particle energies of the two lowest spin-split LLs ($n=0, \sigma = \pm 1$) are written as

$$E_{0,k_x,\pm 1}^F = \frac{\hbar\tilde{\omega}}{2} \mp \frac{|g_0|\mu_B B}{2} + \frac{\hbar^2}{2m^*} \left(\frac{\Omega}{\tilde{\omega}} \right)^2 k_x^2 - \frac{e^2}{\pi\epsilon} \int_{k_x - k_{F0}^{(\pm 1)}}^{k_x + k_{F0}^{(\pm 1)}} dx M_a(0, x), \quad (13)$$

where the last term corresponds to the exchange interaction. The function $M_a(0, q_x) = 2^{-1} \exp[-(2a^2 - 1)q_x^2/4] K_0(q_x^2/4)$ for $\Omega^2/\omega_c^2 \rightarrow 0$ (correspondingly, $a \rightarrow 1$) coincides with $M(0, q_x)$, and $k_{F0}^{(\pm 1)}$ is the Fermi wave vector of the spin-split level. Note that for the $\nu = 1$ state of the QW, $k_{F0}^{(-1)} = 0$ as only the ($n=0, \sigma = +1$) LL is occupied, the exchange contribution in $E_{0,k_x,-1}^F$ vanishes. The exchange interaction, given in Eq. (13), coincides with Eq. (10) of Ref. 7 only in the limit $\Omega^2/\omega_c^2 \rightarrow 0$ and it is essentially different for $\Omega/\omega_c \geq 1$, in particular, due to the fact that $a \neq 1$.

Integrating Eq. (13) over k_x from $-k_{F0}^{(\pm 1)}$ to $k_{F0}^{(\pm 1)}$, after taking half of the exchange term to avoid double counting, and then summing the result for these two levels we arrive to the expression for the total energy of the QIDES in QW, per unit of length as

$$\begin{aligned}
 E^{F,\text{tot}}(\lambda) &= \frac{\hbar\tilde{\omega}}{2}n_L - |g_0|\mu_B B\lambda + \frac{\pi^2\hbar^2}{6m^*}\left(\frac{\Omega}{\tilde{\omega}}\right)^2 \\
 &\times \sum_{p=0}^1 \left[\frac{n_L}{2} + (-1)^p\lambda \right]^3 \\
 &- \frac{e^2}{2\pi^2\varepsilon} \sum_{p=0}^1 \int_0^{\pi[n_L/2+(-1)^p\lambda]} dk_x \\
 &\times \int_{k_x-\pi[n_L/2+(-1)^p\lambda]}^{k_x+\pi[n_L/2+(-1)^p\lambda]} dx M_a(0,x), \quad (14)
 \end{aligned}$$

where λ is the linear density asymmetry between the spin-split levels and $k_{F0}^{(\pm 1)} = \pi[n_L/2 \pm \lambda]$. Notice, the p term of last sum of Eq. (14) cannot be reduced to Eqs. (13) and (14) of Ref. 7 for any finite Ω/ω_c . However, for $\Omega^2/\omega_c^2 \ll 1$ the relative difference between them becomes negligible. It is implicit in Eq. (14) that if one spin-split LL is occupied then the condition (i) $E_{0,k_{F0}^{(+1)},+1}^F < \epsilon_{0,0,-1}$ should be satisfied. On the other hand, if both spin-split LLs are occupied then the condition of thermodynamical stability (ii) $E_{0,k_{F0}^{(+1)},+1}^F = E_{0,k_{F0}^{(-1)},-1}^F$ should be satisfied. We note that the conditions (i) and (ii) are actually fulfilled only for one, two or three values of λ within the range $n_L/2 \geq \lambda \geq 0$ depending on ω_c, Ω and other parameters. It does mean that each one of the three curves of Fig. 2 in Ref. 7 (plotted for three values of n_L) are really reduced, due to necessary conditions (i) and (ii), to three points corresponding to $\lambda=0$, $n_L/2$, and a third λ which has a more specific value for each curve.

By applying Eqs. (13) and (14) to GaAs-based QWs of Refs. 10 and 13, with fixed n_L , we obtain that for any $\lambda \in [0, n_L/2]$ the results for the critical magnetic field $B_{\text{cr}}^{(2),F}$ for the actual value of $|g_0|=0.44$ are very close to results for $g_0=0$. Indeed, in Eq. (14), $|g_0|\mu_B B \ll e^2/\varepsilon\tilde{l}$. So in very good approximation we further assume that $g_0=0$.

Our analysis shows that the state with the lowest total energy corresponds to $\lambda=0$ (equally occupied spin-split LLs: $\nu=2$ state) or to $\lambda=n_L/2$ (one occupied spin-split LL: $\nu=1$ state). Then to calculate $B_{\text{cr}}^{(2),F}$, within the second scenario where the $\nu=1$ state with width $W(k_{F0}^{(1)}=k_F, k_{F0}^{(-1)}=0)$ collapses to the $\nu=2$ state with width $W/2(k_{F0}^{(\pm 1)}=k_F/2)$, we need to solve the equation

$$\Delta E^{F,\text{tot}}(B, \Omega; n_L) \equiv E^{F,\text{tot}}(n_L/2) - E^{F,\text{tot}}(0) = 0. \quad (15)$$

For fixed n_L , from Eq. (15), we obtain the critical curve $\Omega(B_{\text{cr}}^{(2),F})$. We point out that the latter curve is different from the equivalent critical curve $\Omega(B_{\text{cr}}^{(2),\text{KL}})$, calculated within the Kinaret-Lee model due to the inappropriate calculation of the exchange interaction term, as outlined above. In contrast with the first scenario discussed in the previous section where, at $B_{\text{cr}}^{(1)}$, there is no change of the effective QW width, now the QW width drops sharply by a factor 2 at a certain $B_{\text{cr}}^{(2),F}$. As a consequence, this strong redistribution of the charge density in the QW compels us to add the Hartree interaction that results in the direct interaction term

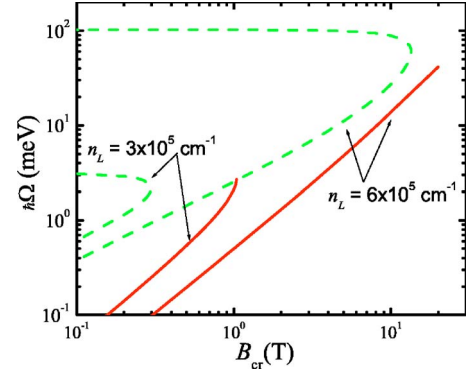


FIG. 7. (Color online.) Critical curves Ω vs B_{cr} for the collapse ($G_a=0$) of the $\nu=1$ state in the GaAs-based QWs, for two linear densities. The first scenario $\Omega=\Omega(B_{\text{cr}}^{(1)})$, shown by the red solid curves, is calculated within the BS approach. The second scenario $\Omega=\Omega(B_{\text{cr}}^{(2)})$, indicated by the green dashed curves, is evaluated in the HFA from Eq. (17).

$$\Delta E^H = \frac{4e^2}{\pi^2\varepsilon a^2\tilde{l}^2} \int_0^\infty \frac{du}{u^3} e^{-u^2/2} \left[1 - \cos^2\left(\frac{ak_F\tilde{l}u}{2}\right) \right]^2, \quad (16)$$

modifying the Eq. (15) and leading to the correct expression for the critical point in the HFA, as

$$\Delta E^{\text{HF,tot}}(B, \Omega; n_L) \equiv \Delta E^{F,\text{tot}}(B, \Omega; n_L) - \Delta E^H = 0. \quad (17)$$

We observe that because $\Delta E^H > 0$, for any finite B , it follows from Eq. (17) that, in the HFA, the Hartree interaction contributes to make the total energy of the $\nu=1$ state lower than that of the $\nu=2$ QW state. We will see that for $\Omega/\omega_c \leq 1$ and n_L, Ω fixed, the critical magnetic field $B_{\text{cr}}^{(2)}$, calculated from Eq. (17), is very different from $B_{\text{cr}}^{(2),F}$, calculated by neglecting the Hartree interaction. It is easy to see that for $\Omega/\omega_c \rightarrow \infty$ the difference between Eqs. (15) and (17) becomes negligible, and $B_{\text{cr}}^{(2),F} \approx B_{\text{cr}}^{(2)}$.

B. Phase diagram for the $\nu=1$ state collapse

The phase diagrams for the collapse of the $\nu=1$ state of the interacting QIDES, laterally confined by a parabolic potential with characteristic frequency Ω , that follow from the first and the second scenarios, are plotted on a logarithmic scale in Fig. 7. The horizontal axis represents the critical magnetic field B_{cr} at which the activation gap is suppressed, while the vertical axis is the confinement frequency on a scale compatible with parameters for GaAs-based samples. The red solid curves represent the suppression of the activation gap, driven by exchange-correlation effects in the QW that are calculated for the proposed first scenario within the BS approach. The green dashed lines are obtained from the solution of Eq. (17) and corresponds to the second scenario where the phase transition due to equal population of both spin-split LLs occurs at $B_{\text{cr}}^{(2)}$.

In Fig. 8 we compare the critical curve Ω vs B_{cr} (red solid line), calculated within the HFA [Eq. (17), for the second scenario with the result obtained from the solution of Eq. (15), or Eq. (17) where the Hartree interaction contribution

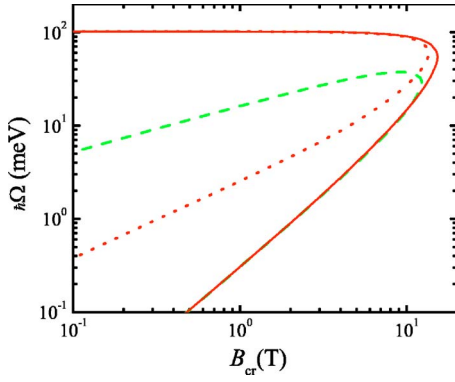


FIG. 8. (Color online.) Comparison of the second scenario result for the critical curve $\Omega = \Omega(B_{\text{cr}}^{(2)})$ plotted by the red solid curve [from Eq. (17)] with the result from the Kinaret and Lee scenario $\Omega = \Omega(B_{\text{cr}}^{(2),\text{KL}})$ plotted by the green dashed curve [from their Eqs. (12)–(14) in which the Hartree interaction is not taken into account (Ref. 7)]. The result of the second scenario with the Hartree interaction discarded, $\Omega = \Omega(B_{\text{cr}}^{(2),F})$, is plotted by the red dotted curve. The linear density for a QW is $n_L = 6 \times 10^5 \text{ cm}^{-1}$.

ΔE^H is excluded (red dotted line). We also show the critical curve $\Omega(B_{\text{cr}}^{(2),\text{KL}})$ calculated for the Kinaret-Lee model, according to the Eqs. (12)–(14) of Ref. 7 (green dashed line).

Critical curves $\Omega(B_{\text{cr}})$ are depicted in Fig. 9 in a linear-scale plot for the experimental conditions of Ref. 13. The curves split the region $\nu=2$ on the left side from the region $\nu=1$ on the right side of the phase diagram. The red solid curve represents $\Omega(B_{\text{cr}}^{(1)})$ for the first scenario calculated in

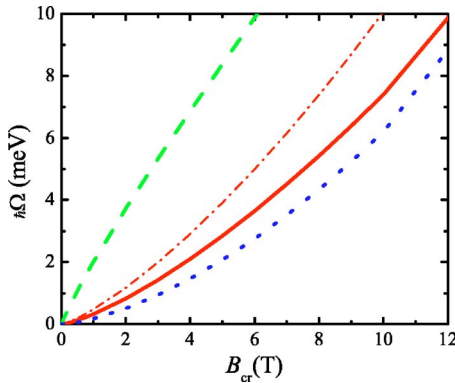


FIG. 9. (Color online.) Linear scale plot of the critical curves for the experimental conditions of Ref. 13, with $n_L = 8.5 \times 10^5 \text{ cm}^{-1}$. The first scenario result, $\Omega = \Omega(B_{\text{cr}}^{(1)})$, calculated in the BS scheme, is given by the red solid curve and the red dot-dashed curve plots, $\Omega = \Omega(B_{\text{cr}}^{(1),\text{HF}})$, the same curve, however, with neglected correlations, i.e., in the HFA. One can see clearly, by comparing these curves, the role of electron correlations. The green dashed line represents the second scenario result, $\Omega = \Omega(B_{\text{cr}}^{(2)})$, in the HFA. The result of the Ref. 7 model, $\Omega = \Omega(B_{\text{cr}}^{(2),\text{KL}})$, is denoted by the blue dotted curve; in Fig. 9 it will practically coincide with our result, $\Omega = \Omega(B_{\text{cr}}^{(2),F})$, for omitted direct interaction in the second scenario. It can be seen that only the red solid curve, obtained within the first scenario, can explain the observed critical magnetic fields in which the collapse of the $\nu=1$ state occurs for different values of Ω as the blue dotted curve should be discarded.

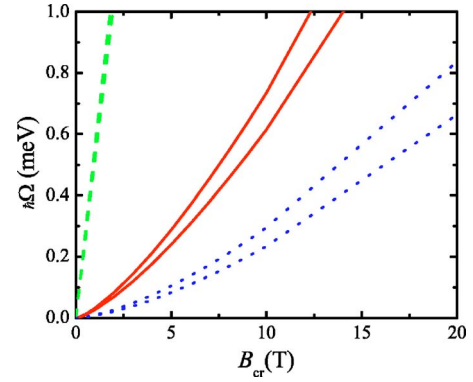


FIG. 10. (Color online.) Same critical curves, as in Fig. 9, for the sample 1 (sample 2) quantum wire of Ref. 10 with $n_L = 7.0(6.0) \times 10^6 \text{ cm}^{-1}$ plotted by the lower (upper) the red solid line, $\Omega = \Omega(B_{\text{cr}}^{(1)})$, the green dashed curve $\Omega = \Omega(B_{\text{cr}}^{(2)})$ and the blue dotted line $\Omega = \Omega(B_{\text{cr}}^{(2),\text{KL}})$. Only the first scenario results explain well the experimental observations¹⁰ (see the text).

the BS approach and the red dot-dashed line shows $\Omega(B_{\text{cr}}^{(1),\text{HF}})$ in the HFA. The comparison between these curves indicates the role of electron correlations in the QW system for the first scenario. The green dashed curve indicates $\Omega(B_{\text{cr}}^{(2)})$ for the second scenario in the HFA [from Eq. (17)] and $\Omega(B_{\text{cr}}^{(2),\text{KL}})$ is depicted by the blue dotted curve. Our results for $\Omega(B_{\text{cr}}^{(2),F})$ [calculated from Eq. (15), but not shown in Fig. 9] coincide with those from Ref. 7, because $\omega_c^2/\Omega^2 \gg 1$ for the curves depicted in Fig. 9.

Various experimental consequences of our theoretical analysis are now discussed. For the lowest confinement frequency $\hbar\Omega = 4.75 \text{ meV}$, taken from the experiment of Ref. 13 for the side gate voltage, which controls the lateral confinement, $V_{\text{side}} = 0$, the predicted critical magnetic fields from curves of Fig. 9 are $B_{\text{cr}}^{(1)} = 7.26 \text{ T}$, and $B_{\text{cr}}^{(2)} = 2.65 \text{ T}$, whereas the experimental value is $B_{\text{cr}} = 7 \text{ T}$. The close agreement is a clear evidence that the first scenario is realized in this case. Note that here $B_{\text{cr}}^{(2),F} \approx B_{\text{cr}}^{(2),\text{KL}} = 8.47 \text{ T}$ and $B_{\text{cr}}^{(1),\text{HF}} = 5.73 \text{ T}$ for $\hbar\Omega = 4.75 \text{ meV}$. For the largest confinement frequency, $\hbar\Omega \approx 7.0 \text{ meV}$, obtained for the largest negative V_{side} in Ref. 13, we have $B_{\text{cr}}^{(1)} = 9.6 \text{ T}$ and $B_{\text{cr}}^{(2)} = 4.1 \text{ T}$ that can be compared with the experimental value $B_{\text{cr}} = 10 \text{ T}$. This allows us to conclude that the first scenario is again realized. Note that for the same confining frequency it follows that $B_{\text{cr}}^{(1),\text{HF}} = 7.7 \text{ T}$ and $B_{\text{cr}}^{(2),F} \approx B_{\text{cr}}^{(2),\text{KL}} = 10.8 \text{ T}$. That is surprising that for some specific values of the confinement frequency, the results taking into account only the exchange interaction can lead to B_{cr} close to the experimental ones, even though, from the theoretical point of view, we have shown that the Hartree direct term is quite essential because the strong redistribution of the electron density in this scenario.

Now we continue our discussion by analyzing the realization of two scenarios for the sample parameters of the older experiment.¹⁰ In Fig. 10, we depict the critical curves $\Omega(B_{\text{cr}}^{(1)})$ and $\Omega(B_{\text{cr}}^{(2)})$ by red solid lines and green dashed lines respectively. We plot also for comparison $\Omega(B_{\text{cr}}^{(2),\text{KL}})$, obtained within the Kinaret-Lee model by the blue dotted lines; there is no noticeable difference between $\Omega(B_{\text{cr}}^{(2),F})$ and $\Omega(B_{\text{cr}}^{(2),\text{KL}})$

in this case. For parameters of sample 1, used in Fig. 1 ($\hbar\Omega=0.65$ meV), we observe that $B_{\text{cr}}^{(1)}=10.8$ T (for $g_0=-0.44$ it should be $B_{\text{cr}}^{(1)}=10.4$ T) and $B_{\text{cr}}^{(2)}=1.27$ T. The other critical fields $B_{\text{cr}}^{(2),\text{KL}}\approx B_{\text{cr}}^{(2),F}=20.0$ T. These results support the occurrence of the first scenario, because the $\nu=1$ state was not observed at $B=10$ T due to its collapse.¹⁰ We see again how important is the Hartree contribution for the stability of the $\nu=1$ state in the second scenario. Furthermore, for the parameters of sample 2 of Ref. 10, used in Fig. 2 ($\hbar\Omega=0.46$ meV), we find $B_{\text{cr}}^{(1)}=7.3$ T (for finite $g_0=-0.44$, it should be $B_{\text{cr}}^{(1)}=7.0$ T), $B_{\text{cr}}^{(2)}=0.82$ T, and $B_{\text{cr}}^{(2),\text{KL}}\approx B_{\text{cr}}^{(2),F}=13.1$ T. In addition, for the parameters used in Fig. 3 ($\hbar\Omega=0.26$ meV) of the same sample, we obtain $B_{\text{cr}}^{(1)}=4.8$ T (notice, for finite $g_0=-0.44$, it should be $B_{\text{cr}}^{(1)}=4.6$ T), $B_{\text{cr}}^{(2)}=0.46$ T, and $B_{\text{cr}}^{(2),\text{KL}}\approx B_{\text{cr}}^{(2),F}=9.2$ T. As for the fixed confinement frequencies in Fig. 10, we concluded that the theoretical results indicate again the occurrence of the first scenario, because the observed $\nu=1$ QHE state persists with the centre of the plateau at $B=7.3$ T.¹⁰

IV. CONCLUSIONS

We have studied in this work two scenarios for phase transitions leading to the collapse of the $\nu=1$ quantum Hall state in a QW due to the suppression of exchange-enhanced activation g factor. In the first scenario the collapse of the activation gap G_a (as well as the g factor) occurs at $B_{\text{cr}}^{(1)}$ without any finite redistribution of the charge density in the QW; we have obtained it for a still strong exchange-enhanced optical g factor $g_{\text{op}}^*(0)$ at the center of the QW (see Fig. 5), which is in reasonable agreement with the experimental results.¹³ Within the second scenario of the collapse of the quantum Hall state, there is a strong decrease of the

electron width W of the QW at $B_{\text{cr}}^{(2)}$. In this case $g_{\text{op}}^*(k_x)$ drops to zero for any k_x . Because the electron density is strongly redistributed in a narrow region, the Hartree term of the total energy plays essential role and must be included in the calculations.

We call the attention for an important point coming from our theoretical investigations. In the second scenario, it follows (see Fig. 8, for instance) that, for a given n_L , there is Ω_0 such that for $\Omega>\Omega_0$ and for any B , in particular, for $B\rightarrow 0$, the $\nu=1$ state should be stable. Furthermore, Ω can be chosen sufficiently large so that the parameter $e^2/(\epsilon\tilde{\hbar}\tilde{\omega})$ would be extremely small. However, this contradicts the Lieb-Mattis theorem¹⁶ that assures that the ground state of 1D many-body system is demagnetized.^{17,18} This result reinforces the role of correlations for weak magnetic fields.

Our study, using the extended BS approach, demonstrated the importance to take into account correlation effects, due to edge states screening, for the dependence of the LLs on the position nearby the edges. We have compared the theoretical results in both scenarios with experiments performed by two different groups.^{10,13} Even though a direct comparison with experiments should be difficult, due to different samples and accuracy of essential parameters, our overall conclusion is that the first scenario is most favorable to be realized in QWs.

ACKNOWLEDGMENTS

This work was supported in part by Fundação de Amparo à Pesquisa do Estado de São Paulo (FAPESP). One of the authors (S.S.) is grateful to Coordenação de Aperfeiçoamento de Pessoal de Nível Superior (CAPES) for financial support and to Universidade do Amazonas for a leave of absence. N.S. acknowledges Conselho Nacional de Desenvolvimento Científico e Tecnológico (CNPq).

*Electronic address: vbalev@df.ufscar.br

¹D. B. Chklovskii, B. I. Shklovskii, and L. I. Glazman, Phys. Rev. B **46**, 4026 (1992).
²G. Muller, D. Weiss, A. V. Khaetskii, K. von Klitzing, S. Koch, H. Nickel, W. Schlapp, and R. Losch, Phys. Rev. B **45**, 3932 (1992).
³J. Dempsey, B. Y. Gelfand, and B. I. Halperin, Phys. Rev. Lett. **70**, 3639 (1993); Surf. Sci. **305**, 166 (1994).
⁴B. Y. Gelfand and B. I. Halperin, Phys. Rev. B **49**, 1862 (1994).
⁵O. G. Balev and Nelson Studart, Phys. Rev. B **64**, 115309 (2001).
⁶I. O. Baleva, Nelson Studart, and O. G. Balev, Phys. Rev. B **65**, 073305 (2002).
⁷J. M. Kinaret and P. A. Lee, Phys. Rev. B **42**, 11 768 (1990).
⁸L. Brey, J. J. Palacios, and C. Tejedor, Phys. Rev. B **47**, 13 884 (1993).
⁹T. Suzuki and Tsuneya Ando, J. Phys. Soc. Jpn. **62**, 2986 (1993).
¹⁰J. Wrobel, F. Kuchar, K. Ismail, K. Y. Lee, H. Nickel, W. Schlapp, G. Grobecki, and T. Dietl, Surf. Sci. **305**, 615 (1994).

¹¹O. G. Balev and P. Vasilopoulos, Phys. Rev. B **56**, 6748 (1997).
¹²Zhongxi Zhang and P. Vasilopoulos, J. Phys.: Condens. Matter **13**, 1539 (2001).
¹³I. Pallecchi, Ch. Heyn, J. Lohse, B. Kramer, and W. Hansen, Phys. Rev. B **65**, 125303 (2002).
¹⁴Zhongxi Zhang and P. Vasilopoulos, Phys. Rev. B **66**, 205322 (2002).
¹⁵In previous works, this approach was called as the generalized local-density approximation (GLDA) in the sense that the results are obtained from a single-particle Schrödinger equation with an effective self-consistent potential which goes beyond the usual LDA. However, the approach clearly takes *nonlocal* effects into account.
¹⁶E. Lieb and D. Mattis, Phys. Rev. **125**, 164 (1962).
¹⁷O. A. Starykh and D. L. Maslov, Phys. Rev. Lett. **82**, 2999 (1999).
¹⁸O. P. Sushkov, Phys. Rev. B **67**, 195318 (2003).